



**CHALMERS**  
UNIVERSITY OF TECHNOLOGY

## **Topological insulator nanoribbon Josephson junctions: Evidence for size effects in transport properties**

Downloaded from: <https://research.chalmers.se>, 2025-07-03 06:13 UTC

Citation for the original published paper (version of record):

Kunakova, G., Pullukattuthara Surendran, A., Montemurro, D. et al (2020). Topological insulator nanoribbon Josephson junctions: Evidence for size effects in transport properties. *Journal of Applied Physics*, 128(19). <http://dx.doi.org/10.1063/5.0022126>

N.B. When citing this work, cite the original published paper.

# Topological insulator nanoribbon Josephson junctions: Evidence for size effects in transport properties

Cite as: J. Appl. Phys. **128**, 194304 (2020); <https://doi.org/10.1063/5.0022126>

Submitted: 17 July 2020 . Accepted: 09 November 2020 . Published Online: 20 November 2020

 Gunta Kunakova, Ananthu P. Surendran,  Domenico Montemurro,  Matteo Salvato, Dmitry Golubev, Jana Andzane, Donats Erts, Thilo Bauch, and  Floriana Lombardi

## COLLECTIONS

Paper published as part of the special topic on [2D Quantum Materials: Magnetism and Superconductivity](#)



View Online



Export Citation



CrossMark

## ARTICLES YOU MAY BE INTERESTED IN

[High transparency Bi<sub>2</sub>Se<sub>3</sub> topological insulator nanoribbon Josephson junctions with low resistive noise properties](#)

Applied Physics Letters **115**, 172601 (2019); <https://doi.org/10.1063/1.5123554>

[A perspective on semiconductor-based superconducting qubits](#)

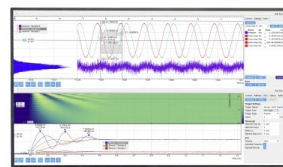
Applied Physics Letters **117**, 240501 (2020); <https://doi.org/10.1063/5.0024124>

[Characterization of ferroelectric domain walls by scanning electron microscopy](#)

Journal of Applied Physics **128**, 191102 (2020); <https://doi.org/10.1063/5.0029284>

Challenge us.

What are your needs for periodic signal detection?



Zurich  
Instruments

# Topological insulator nanoribbon Josephson junctions: Evidence for size effects in transport properties

Cite as: J. Appl. Phys. **128**, 194304 (2020); doi: [10.1063/5.0022126](https://doi.org/10.1063/5.0022126)

Submitted: 17 July 2020 · Accepted: 9 November 2020 ·

Published Online: 20 November 2020



Gunta Kunakova,<sup>1,2</sup>  Ananthu P. Surendran,<sup>1</sup> Domenico Montemurro,<sup>1,3</sup>  Matteo Salvato,<sup>4</sup>  Dmitry Golubev,<sup>5</sup> Jana Andzane,<sup>2</sup> Donats Erts,<sup>2</sup> Thilo Bauch,<sup>1</sup> and Floriana Lombardi<sup>1,a)</sup> 

## AFFILIATIONS

<sup>1</sup>Quantum Device Physics Laboratory, Department of Microtechnology and Nanoscience, Chalmers University of Technology, SE-41296 Göteborg, Sweden

<sup>2</sup>Institute of Chemical Physics, University of Latvia, Raina Blvd. 19, LV-1586 Riga, Latvia

<sup>3</sup>Dipartimento di Fisica “Ettore Pancini,” Università degli Studi di Napoli Federico II, I-80125 Napoli, Italy

<sup>4</sup>Dipartimento di Fisica, Università di Roma “Tor Vergata,” 00133 Roma, Italy

<sup>5</sup>QTF Centre of Excellence, Department of Applied Physics, Aalto University, P.O. Box 15100, FI-00076 Aalto, Finland

**Note:** This paper is part of the Special Topic on 2D Quantum Materials: Magnetism and Superconductivity

**a)** Author to whom correspondence should be addressed: [floriana.lombardi@chalmers.se](mailto:floriana.lombardi@chalmers.se)

## ABSTRACT

We have used Bi<sub>2</sub>Se<sub>3</sub> nanoribbons, grown by catalyst-free physical vapor deposition to fabricate high quality Josephson junctions with Al superconducting electrodes. In our devices, we observe a pronounced reduction of the Josephson critical current density  $J_c$  by reducing the width of the junction, which in our case corresponds to the width of the nanoribbon. Because the topological surface states extend over the entire circumference of the nanoribbon, the superconducting transport associated with them is carried by modes on both the top and bottom surfaces of the nanoribbon. We show that the  $J_c$  reduction as a function of the nanoribbon width can be accounted for by assuming that only the modes traveling on the top surface contribute to the Josephson transport as we derive by geometrical consideration. This finding is of great relevance for topological quantum circuitry schemes since it indicates that the Josephson current is mainly carried by the topological surface states.

© 2020 Author(s). All article content, except where otherwise noted, is licensed under a Creative Commons Attribution (CC BY) license (<http://creativecommons.org/licenses/by/4.0/>). <https://doi.org/10.1063/5.0022126>

## I. INTRODUCTION

The study of the proximity effect between a superconductor and a semiconductor or an unconventional metal has lately received a dramatic boost due to the increasing possibilities to manufacture a larger variety of interfaces and materials. Novel phenomenology of the proximity effect is currently coming from the integration of semiconducting nanowires, with strong spin-orbit coupling, as barriers, as well as the edge and surface states of two-dimensional (2D) and three-dimensional (3D) Topological Insulators (TIs)<sup>1–5</sup> and Dirac semimetals.<sup>6,7</sup> In these cases, the Josephson transport properties of the hybrid devices will manifest neat fingerprints related to the formation of Majorana bound

states, which is of great interest for topological quantum computation.<sup>8–10</sup> Lately, superconductor–TI–superconductor Josephson junctions with 2D and 3D TIs have shown a  $4\pi$  periodic Josephson current phase relations,<sup>11–14</sup> which could be associated with the presence of Majorana modes<sup>15</sup> and gate-tunable Josephson effects<sup>2,16–19</sup> when the TI is tuned through the TI's Dirac point. Still several aspects of the physics of the Josephson effect related to the topological protected edge/surface states and the contribution of the unavoidable bulk remain to be clarified. In this respect, the use of 3D TI nanoribbons could be advantageous because of the reduced number of transport channels involved in the transport. Here, the transport is ruled by the quantization of

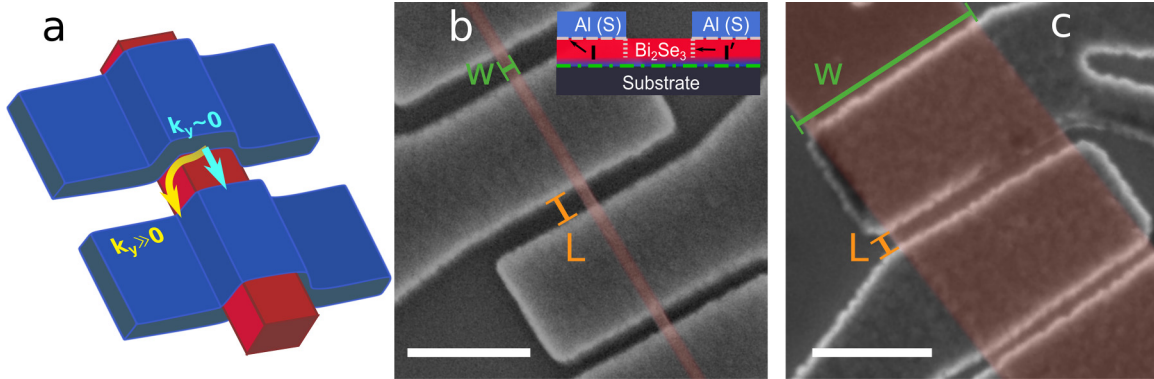


**FIG. 1.** (a) Schematics of a  $\text{Bi}_2\text{Se}_3$  nanoribbon Josephson junction. Arrows indicate transport modes carrying supercurrent by the topological surface states at the nanoribbon top surface ( $k_y \sim 0$ ) and around the perimeter ( $k_y \gg 0$ ). (b) and (c) Partly colored SEM images of the fabricated Josephson junctions of  $\text{Bi}_2\text{Se}_3$  nanoribbons with different widths  $W$ .  $L$  indicates the length of a junction. The scale bar is 500 nm. The inset in panel (b) is a schematic cross section of a junction, and the dotted-dashed green line highlights the location of a trivial 2DEG.<sup>20</sup>

the nanoribbon's propagation modes, which could give new hints about the Josephson phenomenology associated with the Topological Surface States (TSSs).

In this work, we have fabricated Josephson junctions by using  $\text{Bi}_2\text{Se}_3$  Topological Insulator Nanoribbons (TINRs) with widths spanning from 50 nm to almost a micron. Because the TSSs extend over the entire circumference of the TINR, the superconducting transport associated with them is carried by modes on both the top and bottom surface of the nanoribbon. As shown in Fig. 1(a), in our TINR Josephson junction, the current flows between the superconducting contacts fabricated on the top surface of the nanoribbon. For the TINR with a circumference of  $C = 2W + 2t$  (where  $W$  is the width and  $t$  the thickness of the nanoribbon), the transverse momentum  $k_y$ , perpendicular to the current (see Fig. 1), is quantized as

$$k_y = 2\pi(n + 1/2)/C, \quad (1)$$

where  $n$  is an integer.<sup>21</sup> Therefore, the modes with  $k_y \sim 0$  remain on the top surface, while the modes with  $k_y \gg 0$  are winding around the perimeter of the TINR [see Fig. 1(a)]. Here, we show that the value of the Josephson current density strongly depends on the junction width, which in our case corresponds to the width of the nanoribbons [Fig. 1(a)]. We discuss the possible origin of this phenomenology also in connection with the fact that only small  $k_y$  value modes are involved in the Josephson transport, which are the ones that travel on the top surface of the nanoribbon. This number reduces by reducing the nanoribbon width [see Eq. (1)]. This finding is of great relevance since it indicates that (a) the Josephson current is mainly carried by the surface states and (b) because of the selectivity in  $k_y$ , the number of modes involved in the transport scales much faster compared to the width. This is of great relevance for topological quantum circuitry schemes.

## II. EXPERIMENTAL DETAILS AND RESULTS

Nanoribbons of  $\text{Bi}_2\text{Se}_3$  with a variation of widths from  $\sim 50$  nm to about  $1 \mu\text{m}$  were grown as reported in Ref. 22. For the fabrication of Josephson junctions, nanoribbons were transferred to pre-patterned substrates of Si/300 nm  $\text{SiO}_2$  and  $\text{SrTiO}_3$  (STO). We used two different TINR growth batches for the two substrates, respectively. For the two batches, the carrier densities of the topological surface states measured through Shubnikov-de Haas oscillations varied by a factor of 2.<sup>22</sup> A standard process of electron beam lithography was used, followed by the evaporation of 3 and 80 nm thick layers of Pt and Al, respectively. Before the evaporation of the metals, the samples were etched for 30 s by Ar ion milling to remove the native oxide layer of the nanoribbons. SEM images of the fabricated Al/ $\text{Bi}_2\text{Se}_3$ /Al Josephson junctions for different nanoribbon widths are shown in Figs. 1(b) and 1(c). The Pt interlayer between the  $\text{Bi}_2\text{Se}_3$  and Al has an important role in the formation of a transparent interface, as it was shown in our previous works.<sup>3,23,24</sup>

Junctions were measured at a base temperature of 19 mK in an  $rf$ -filtered dilution refrigerator. The planar Josephson junction can be described as  $\text{SIS}'\text{I}'\text{-N-I}'\text{S}'\text{IS}$ . Here,  $\text{S}'$  is the proximized TINR that lies underneath the superconductor (S)—Al, and N represents the not-covered TINR part between the two Al electrodes [see schematics in the inset of Fig. 1(b)]. I is the interface of the barrier between the Al and the  $\text{Bi}_2\text{Se}_3$  nanoribbon, while  $\text{I}'$  represents the barrier interface formed between the  $\text{Bi}_2\text{Se}_3$  under the Al and the  $\text{Bi}_2\text{Se}_3$  of the normal metal region N (nanogap). We have previously demonstrated that both I and  $\text{I}'$  are highly transparent<sup>3,23</sup> and that we have full control of the strength and phenomenology of the proximity effect. When the voltage drop across the Al/ $\text{Bi}_2\text{Se}_3$  interface is negligible, compared to that across the TI in the nanogap, as in our case,<sup>25</sup> the physics of the planar junction is effectively that of a  $\text{S}'\text{I}'\text{-N-I}'\text{S}'$ .

A typical current-voltage characteristic (IVC) of one of the TINR based Josephson junctions is shown in Fig. 2(a). The IVCs of

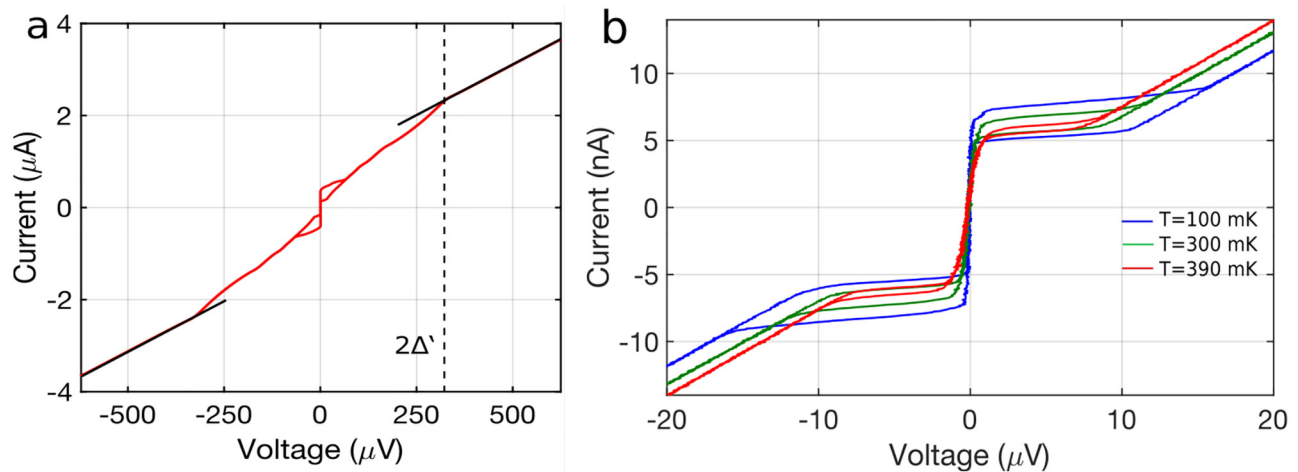


**FIG. 2.** (a) Current–voltage characteristic of a  $\text{Bi}_2\text{Se}_3$  nanoribbon junction ( $I_c = 0.36 \mu\text{A}$ ,  $L = 70 \text{ nm}$ ,  $t = 16 \text{ nm}$ ,  $W = 430 \text{ nm}$ ) measured at  $T = 20 \text{ mK}$ . The solid black lines are linear fits of the IVC at high bias voltages. The departure from linearity observed at  $V = 340 \mu\text{V}$  corresponds to twice the induced gap, with gap  $\Delta' = 170 \mu\text{V}$  (see the dashed line). (b) Low bias current–voltage characteristics at various temperatures  $T = 100, 300,$  and  $390 \text{ mK}$  of a  $\text{Bi}_2\text{Se}_3$  nanoribbon junction ( $I_c = 10 \text{ nA}$ ,  $L = 70 \text{ nm}$ ,  $t = 13 \text{ nm}$ ,  $W = 60 \text{ nm}$ ). The hysteretic current–voltage characteristics develop a finite resistance in the superconducting branch for increasing temperature.

our junctions have a hysteresis that points to an increased electron temperature as the junction is switched to the resistive state.<sup>26</sup> A clear gap structure is seen at  $2\Delta'$  (where  $\Delta'$  is the induced gap of the order of  $170 \mu\text{V}$ ); several bumps in the IVC at  $2\Delta'/n$  are also visible: as we have previously demonstrated they are connected to multiple Andreev reflections that are made possible by the high transparency of the I and I' barriers.<sup>23</sup> The IVCs measured at various temperatures are shown in Fig. 2(b). At higher temperatures, we observe a finite resistance in the supercurrent branch. This could be attributed to premature switching and consecutive retrapping of the superconducting phase difference.<sup>27–30</sup> The so-called phase diffusion regime is characteristic for a moderate to low quality phase Josephson junction. The quality factor can be estimated using  $Q = \omega_p RC$ , with the plasma frequency  $\omega_p = \sqrt{2\pi I_c / \Phi_0 C}$ , where  $\Phi_0 = h/2e$  is the superconductive flux quantum, and  $R \simeq 100 \Omega$  is the real part of the shunting admittance of a dc biased Josephson junction.<sup>31,32</sup> Here, the capacitance is dominated by the shunting capacitance through the substrate. For STO with a relative dielectric constant of 25 000 at low temperatures, we approximate  $C \simeq 1 \text{ pF}$  resulting in a quality factor smaller than one for junctions having a critical current lower than 50 nA. Alternatively, for the Si/SiO<sub>2</sub> substrate, it is more difficult to estimate the shunting capacitance due to the conducting substrate. However, we expect a much smaller capacitance value resulting in quality factors smaller than one for critical currents already below 500 nA.

The value of the critical current of the junction  $I_c$  is obtained from the forward scan, and the critical current density  $J_c$  is calculated accordingly by dividing  $I_c$  by the width of the nanoribbon ( $W$ ). The normal state resistance  $R_N$  is determined by the inverse of the slope, calculated from the IVC region at voltages above  $2\Delta'$  in S' (represented by the area of  $\text{Bi}_2\text{Se}_3$  underneath the Al).

Figures 3(a) and 3(b) show the dependence of the  $J_c$  as a function of the  $W$  for devices with different lengths  $L$  fabricated on Si/SiO<sub>2</sub> and STO substrates, respectively. In Fig. 3(b), we have included a  $10 \mu\text{m}$  wide junction where the Al electrodes are patterned along the length of TINR; for this device, no winding modes are expected to contribute to the Josephson transport. One

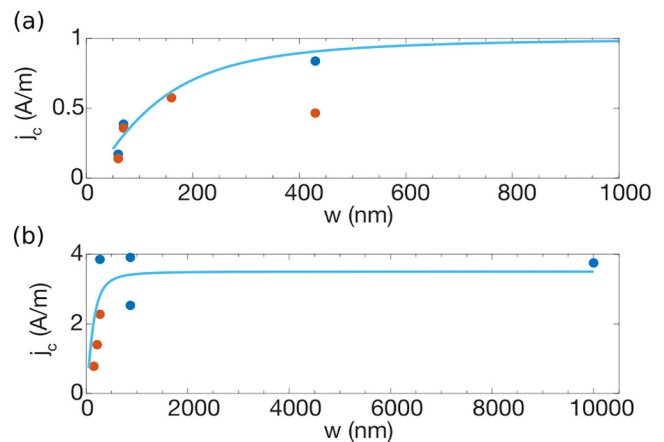


**FIG. 3.** (a) Critical current density as a function of TINR width for Josephson junction devices realized from the same growth batch on a Si/SiO<sub>2</sub> substrate. (b) Critical current density as a function of TINR width for Josephson junctions realized from a second growth batch [different from those shown in panel (a)] on a SrTiO<sub>3</sub> substrate. All measurements were performed at  $T = 20 \text{ mK}$ . The blue and red dots are for junction lengths of 50–80 nm and 100–110 nm, respectively.

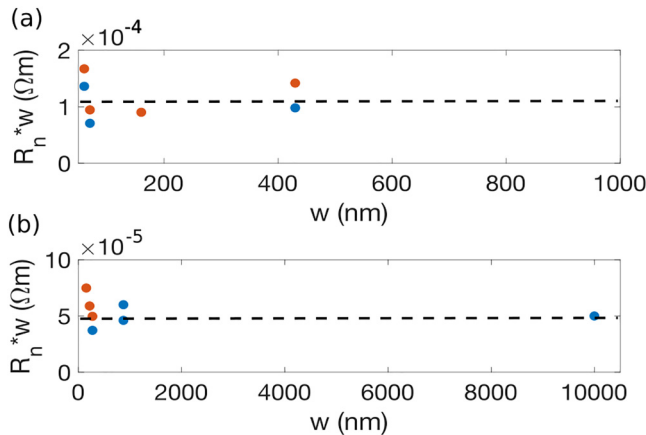


**FIG. 4.** (a) Specific resistance as a function of TINR width for Josephson junction devices realized from the same growth batch on a Si/SiO<sub>2</sub> substrate. (b) Specific resistance as a function of TINR width for Josephson junctions realized from a second growth batch [different from those shown in panel (a)] on a SrTiO<sub>3</sub> substrate. All measurements were performed at  $T = 20$  mK. The blue and red dots are for junction lengths of 50–80 nm and 100–110 nm, respectively.

clearly sees that if the length is fixed, the  $J_c$  sharply decreases as a function of the width  $W$  of the nanoribbon. We note that the value of  $J_c$  can change by a factor of 5–6 by going from the narrowest nanoribbons of 60 nm to the widest ones. In contrast, as shown in Figs. 4(a) and 4(b), the specific resistance, obtained by considering the product  $R_N \times (W)$  for the devices on the Si/SiO<sub>2</sub> and STO substrate, respectively, is almost independent of  $W$ . This fact allows one to exclude that the reduction of the  $J_c$  at small widths  $W$  has its origin in strong modifications/deterioration of the junction specific resistance for narrow TINR.

### III. DISCUSSION AND CONCLUSIONS

What is the origin of this peculiar  $J_c(W)$  phenomenology? As we have discussed earlier, the explanation of the phenomenon can have its ground in the quantization of the nanoribbon’s propagation modes. One can derive that the relative number of modes  $n_{top}/n_{tot}$  traveling only on the top surface reduces with the junction width for a fixed junction length  $L$ . Here,  $n_{tot}$  is the total number of modes,

$$n_{tot} = k_F C / 2\pi - 1/2, \quad (2)$$

and  $n_{top}$  is the number of modes traveling only on the top surface of the nanoribbon,

$$n_{top} = k_F C W / 4\pi L ((W/2L)^2 + 1)^{-1/2} - 1/2. \quad (3)$$

The relations above can be obtained from geometric considerations; see Fig. 5(a). Here,  $k_F$  is the Fermi vector.

In Fig. 5(b), we show the width dependence of the relative number of modes  $n_{top}/n_{tot}$  for three different junction lengths.

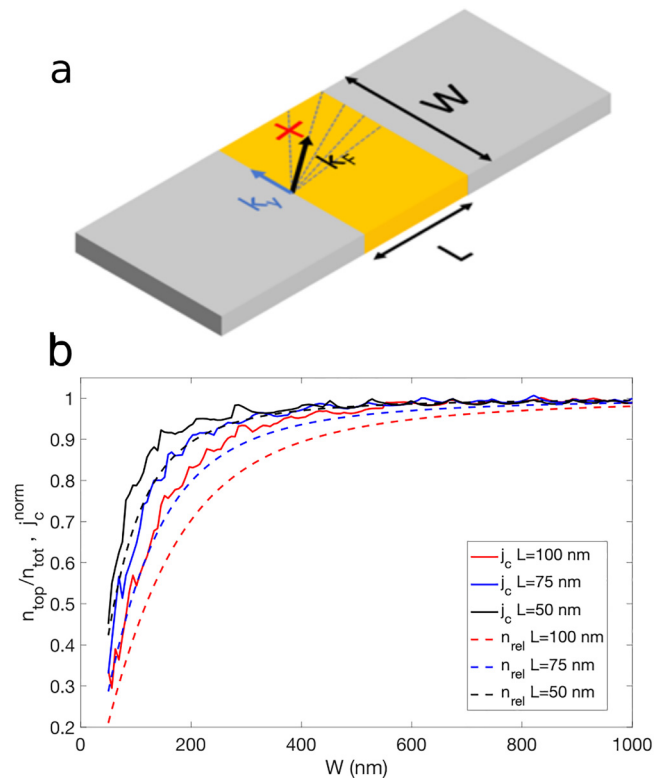


**FIG. 5.** (a) Sketch of a planar TI junction with electrode separation  $L$  and width  $W$ . The dashed lines indicate quasiparticle trajectories. The maximum transversal momentum for which the transport mode still propagates only on the top surface is indicated by  $k_y$ . For larger transversal momentum, the quasiparticle trajectory has to wind around the TINR and does not contribute to the critical current (red cross). (b) Relative number of transport modes  $n_{rel} = n_{top}/n_{tot}$  propagating only on the top surface (dashed lines) and the corresponding normalized critical current density (solid lines) as a function of junction width for three different junction lengths.

The curves of Fig. 5(b) have been obtained by considering  $k_F = 0.55 \text{ nm}^{-1}$ , a value that is typical for our nanoribbons.<sup>20</sup> For  $L = 100$  nm, we obtain a reduction of the relative number of modes traveling only on the top surface by a factor of 5 when reducing the junction width going from 900 nm to 50 nm.

For comparison in Fig. 5, we also show the full calculation of the supercurrent density following Ref. 7 taking into consideration also the angle dependence of the transmission coefficients of each transport mode traveling only on the top surface. We see that the full calculation of  $J_c$  and the relative number of transport modes using Eqs. (2) and (3) give the same qualitative behavior.

This dependency qualitatively reproduces the measured  $J_c$  vs width dependence shown in Figs. 3(a) and 3(b). Indeed, the solid lines represent the relative number of transport modes for  $L = 100$  nm. This suggests that only the modes traveling on the top surface contribute to the Josephson current. We note that the critical current density of the  $10 \mu\text{m}$  wide device is in agreement with

the saturation value of the expected current density, where the contribution of winding modes to the total Josephson current is negligible.

A possible explanation for this finding could be related to the lower mobility of the Dirac states at the interface between the TINR and the substrate. Indeed, our magnetotransport measurements have shown the formation of a trivial 2D gas at the interface with the substrate overlapping with the Dirac states at the nanoribbon bottom [see the inset of Fig. 1(b)].<sup>20</sup> This interaction, which leads to a lower mobility (diffusive transport regime) of the Dirac states, might be responsible for the transport modes winding around the nanoribbon (high  $k_y$  modes) contributing less to the Josephson transport. Although we cannot exclude that the transport through the trivial 2D gas contributes to the Josephson current, it would only cause a constant offset of the  $J_C$  values without affecting the overall width dependence. We observe that the overall values of  $J_C$  for the devices on the STO substrate are higher than those on Si/SiO<sub>2</sub>. This can be partially attributed to the larger values of the top surface Dirac carrier density of the batch used to realize the devices on the STO substrate. The larger value of the trivial 2D carrier density we typically observe in devices fabricated on STO substrates<sup>33</sup> could be further responsible for the difference observed in the critical current densities between devices on STO and Si/SiO<sub>2</sub> substrates.

To conclude, we have fabricated high transparency 3D TINR Josephson junctions showing a peculiar phenomenology that can be associated with the transport through the topological surface states. This is a step forward toward the study of topological superconductivity in a few mode devices instrumental for topological quantum computation.

## ACKNOWLEDGMENTS

This work has been supported by the European Union's Horizon 2020 Research and Innovation Program (Grant Agreement No. 766714/HiTIME) and by the European Union's project NANOCOHYBRI (Cost Action CA 16218). G.K. acknowledges the European Regional Development Fund project (No. 1.1.1.2/VIAA/1/16/198). This work was supported by the European Union H2020 under the Marie Curie Actions (No. 766025-QuESTech).

## DATA AVAILABILITY

The data that support the findings of this study are available from the corresponding author upon reasonable request.

## REFERENCES

- <sup>1</sup>J. Hajer, M. Kessel, C. Brüne, M. P. Stehno, H. Buhmann, and L. W. Molenkamp, "Proximity-induced superconductivity in CdTe–HgTe core-shell nanowires," *Nano Lett.* **19**, 4078–4082 (2019).
- <sup>2</sup>L. A. Jauregui, M. Kayyalha, A. Kazakov, I. Miotkowski, L. P. Rokhinson, and Y. P. Chen, "Gate-tunable supercurrent and multiple Andreev reflections in a superconductor-topological insulator nanoribbon-superconductor hybrid device," *Appl. Phys. Lett.* **112**, 093105 (2018).
- <sup>3</sup>S. Charpentier, L. Galletti, G. Kunakova, R. Arpaia, Y. Song, R. Baghdadi, S. M. Wang, A. Kalaboukhov, E. Olsson, F. Tafuri, D. Golubev, J. Linder,

T. Bauch, and F. Lombardi, "Induced unconventional superconductivity on the surface states of Bi<sub>2</sub>Te<sub>3</sub> topological insulator," *Nat. Commun.* **8**, 096407 (2017).

<sup>4</sup>L. Galletti, S. Charpentier, M. Iavarone, P. Lucignano, D. Massarotti, R. Arpaia, Y. Suzuki, K. Kadowaki, T. Bauch, A. Tagliacozzo, F. Tafuri, and F. Lombardi, "Influence of topological edge states on the properties of Al/Bi<sub>2</sub>Se<sub>3</sub>/Al hybrid Josephson devices," *Phys. Rev. B: Condens. Matter Mater. Phys.* **89**, 134512–9 (2014).

<sup>5</sup>V. S. Stolyarov, D. S. Yakovlev, S. N. Kozlov, O. V. Skryabina, D. S. Lvov, A. I. Gumarov, O. V. Emelyanova, P. S. Dzhumayev, I. V. Shchetinin, R. A. Hovhannisyanyan, S. V. Egorov, A. M. Kokotin, W. V. Pogosov, V. V. Ryazanov, M. Y. Kupriyanov, A. A. Golubov, and D. Roditchev, "Josephson current mediated by ballistic topological states in Bi<sub>2</sub>Te<sub>2.3</sub>Se<sub>0.7</sub> single nanocrystals," *Commun. Mater.* **1**, 38 (2020).

<sup>6</sup>C. Z. Li, C. Li, L. X. Wang, S. Wang, Z. M. Liao, A. Brinkman, and D. P. Yu, "Bulk and surface states carried supercurrent in ballistic Nb-Dirac semimetal Cd<sub>3</sub>As<sub>2</sub> nanowire-Nb junctions," *Phys. Rev. B* **97**, 115446–8 (2018).

<sup>7</sup>C. Li, J. C. de Boer, B. de Ronde, S. V. Ramankutty, E. van Heumen, Y. Huang, A. de Visser, A. A. Golubov, M. S. Golden, and A. Brinkman, "4 $\pi$ -periodic Andreev bound states in a Dirac semimetal," *Nat. Mater.* **17**, 875–880 (2018).

<sup>8</sup>L. Fu and C. L. Kane, "Superconducting proximity effect and majorana fermions at the surface of a topological insulator," *Phys. Rev. Lett.* **100**, 096407 (2008).

<sup>9</sup>C. Nayak, S. H. Simon, A. Stern, M. Freedman, and S. Das Sarma, "Non-Abelian anyons and topological quantum computation," *Rev. Mod. Phys.* **80**, 1083–1159 (2008).

<sup>10</sup>G.-Y. Huang and H. Q. Xu, "Majorana fermions in topological-insulator nanowires: From single superconducting nanowires to Josephson junctions," *Phys. Rev. B: Condens. Matter Mater. Phys.* **95**, 155420–6 (2017).

<sup>11</sup>J. Wiedenmann, E. Bocquillon, R. S. Deacon, S. Hartinger, O. Herrmann, T. M. Klapwijk, L. Maier, C. Ames, C. Brune, C. Gould, A. Oiwa, K. Ishibashi, S. Tarucha, H. Buhmann, and L. W. Molenkamp, "4 $\pi$ -periodic Josephson supercurrent in HgTe-based topological Josephson junctions," *Nat. Commun.* **7**, 10303 (2016).

<sup>12</sup>L. P. Rokhinson, X. Liu, and J. K. Furdyna, "The fractional a.c. Josephson effect in a semiconductor-superconductor nanowire as a signature of majorana particles," *Nat. Phys.* **8**, 795–799 (2012).

<sup>13</sup>K. L. Calvez, L. Veyrat, F. Gay, P. Plaindoux, C. Winkelmann, H. Courtois, and B. Sacépé, "Joule overheating poisons the fractional ac Josephson effect in topological Josephson junctions," *Commun. Phys.* **2**, 4 (2018).

<sup>14</sup>P. Schüfflgen, D. Rosenbach, C. Li, T. W. Schmitt, M. Schlenvoigt, A. R. Jalil, S. Schmitt, J. Közler, M. Wang, B. Bennemann, U. Parlak, L. Kibkalo, S. Trellenkamp, T. Grap, D. Meertens, M. Luysberg, G. Mussler, E. Berenschot, N. Tas, A. A. Golubov, A. Brinkman, T. Schäpers, and D. Grützmacher, "Selective area growth and stencil lithography for in situ fabricated quantum devices," *Nat. Nanotechnol.* **14**, 825–831 (2019).

<sup>15</sup>F. Domínguez, F. Hassler, and G. Platero, "Dynamical detection of majorana fermions in current-biased nanowires," *Phys. Rev. B: Condens. Matter Mater. Phys.* **86**, 140503 (2012).

<sup>16</sup>M. P. Stehno, P. Ngabonziza, H. Myoren, and A. Brinkman, "Josephson effect and charge distribution in thin Bi<sub>2</sub>Te<sub>3</sub> topological insulators," *Adv. Mater.* **32**, 1908351–6 (2019).

<sup>17</sup>S. Ghatak, O. Breunig, F. Yang, Z. Wang, A. A. Taskin, and Y. Ando, "Anomalous Fraunhofer patterns in gated Josephson junctions based on the bulk-insulating topological insulator BiSbTeSe<sub>2</sub>," *Nano Lett.* **18**, 5124–5131 (2018).

<sup>18</sup>M. Kayyalha, M. Kargarian, A. Kazakov, I. Miotkowski, V. M. Galitski, V. M. Yakovenko, L. P. Rokhinson, and Y. P. Chen, "Anomalous low-temperature enhancement of supercurrent in topological-insulator nanoribbon Josephson junctions: Evidence for low-energy Andreev bound states," *Phys. Rev. Lett.* **122**, 047003 (2017).

<sup>19</sup>S. Cho, B. Dellabetta, A. Yang, J. Schneeloch, Z. Xu, T. Valla, G. Gu, M. J. Gilbert, and N. Mason, "Symmetry protected Josephson supercurrents in three-dimensional topological insulators," *Nat. Commun.* **4**, 1686–1689 (2013).

- <sup>20</sup>G. Kunakova, L. Galletti, S. Charpentier, J. Andzane, D. Erts, F. Léonard, C. D. Spataru, T. Bauch, and F. Lombardi, “Bulk-free topological insulator  $\text{Bi}_2\text{Se}_3$  nanoribbons with magnetotransport signatures of Dirac surface states,” *Nanoscale* **10**, 19595–19602 (2018).
- <sup>21</sup>L. A. Jauregui, M. T. Pettes, L. P. Rokhinson, L. Shi, and Y. P. Chen, “Magnetic field-induced helical mode and topological transitions in a topological insulator nanoribbon,” *Nat. Nanotechnol.* **11**, 345–351 (2016).
- <sup>22</sup>J. Andzane, G. Kunakova, S. Charpentier, V. Hrkac, L. Kienle, M. Baitimirova, T. Bauch, F. Lombardi, and D. Erts, “Catalyst-free vapour-solid technique for deposition of  $\text{Bi}_2\text{Te}_3$  and  $\text{Bi}_2\text{Se}_3$  nanowires/nanobelts with topological insulator properties,” *Nanoscale* **7**, 15935–15944 (2015).
- <sup>23</sup>G. Kunakova, T. Bauch, E. Tralbaldo, J. Andzane, D. Erts, and F. Lombardi, “High transparency  $\text{Bi}_2\text{Se}_3$  topological insulator nanoribbon Josephson junctions with low resistive noise properties,” *Appl. Phys. Lett.* **115**, 172601–5 (2019).
- <sup>24</sup>L. Galletti, S. Charpentier, Y. Song, D. Golubev, S. M. Wang, T. Bauch, and F. Lombardi, “High-transparency  $\text{Al}/\text{Bi}_2\text{Te}_3$  double-barrier heterostructures,” *IEEE Trans. Appl. Supercond.* **27**, 1800404–4 (2017).
- <sup>25</sup>B. Aminov, A. Golubov, and M. Y. Kupriyanov, “Quasiparticle current in ballistic constrictions with finite transparencies of interfaces,” *Phys. Rev. B: Condens. Matter Mater. Phys.* **53**, 365–373 (1996).
- <sup>26</sup>H. Courtois, M. Meschke, J. T. Peltonen, and J. P. Pekola, “Origin of hysteresis in a proximity Josephson junction,” *Phys. Rev. Lett.* **101**, 067002–4 (2008).
- <sup>27</sup>V. M. Krasnov, T. Bauch, S. Intiso, E. Hürfeld, T. Akazaki, H. Takayanagi, and P. Delsing, “Collapse of thermal activation in moderately damped Josephson junctions,” *Phys. Rev. Lett.* **95**, 157002 (2005).
- <sup>28</sup>J. M. Kivioja, T. E. Nieminen, J. Claudon, O. Buisson, F. W. J. Hekking, and J. P. Pekola, “Observation of transition from escape dynamics to underdamped phase diffusion in a Josephson junction,” *Phys. Rev. Lett.* **94**, 247002 (2005).
- <sup>29</sup>D. Massarotti, D. Stornaiuolo, P. Lucignano, L. Galletti, D. Born, G. Rotoli, F. Lombardi, L. Longobardi, A. Tagliacozzo, and F. Tafuri, “Breakdown of the escape dynamics in Josephson junctions,” *Phys. Rev. B* **92**, 054501 (2015).
- <sup>30</sup>L. Longobardi, D. Massarotti, D. Stornaiuolo, L. Galletti, G. Rotoli, F. Lombardi, and F. Tafuri, “Direct transition from quantum escape to a phase diffusion regime in  $\text{YBaCuO}$  biepitaxial Josephson junctions,” *Phys. Rev. Lett.* **109**, 050601 (2012).
- <sup>31</sup>T. Bauch, F. Lombardi, F. Tafuri, A. Barone, G. Rotoli, P. Delsing, and T. Claeson, “Macroscopic quantum tunneling in  $d$ -wave  $\text{YBa}_2\text{Cu}_3\text{O}_{7-\delta}$  Josephson junctions,” *Phys. Rev. Lett.* **94**, 087003 (2005).
- <sup>32</sup>T. Bauch, T. Lindström, F. Tafuri, G. Rotoli, P. Delsing, T. Claeson, and F. Lombardi, “Quantum dynamics of a  $d$ -wave Josephson junction,” *Science* **311**, 57–60 (2006).
- <sup>33</sup>G. Kunakova, T. Bauch, J. Andzane, D. Erts, and F. Lombardi, “High mobility ambipolar magnetotransport in topological insulator  $\text{Bi}_2\text{Se}_3$  nanoribbons” (unpublished).